ELSEVIER

Journal of Biomechanics 41 (2008) 1697–1706

JOURNAL OF BIOMECHANICS

www.elsevier.com/locate/jbiomech
www.JBiomech.com

In vitro hemodynamic investigation of the embryonic aortic arch at late gestation

Kerem Pekkan[a,*], Lakshmi P. Dasi[b], Paymon Nourparvar[b], Srinivasu Yerneni[b], Kimimasa Tobita[c], Mark A. Fogel[d], Bradley Keller[c], Ajit Yoganathan[b]

[a]*Department of Biomedical and Mechanical Engineering, Carnegie Mellon University, PA, USA*
[b]*School of Biomedical Engineering, Georgia Institute of Technology, GA, USA*
[c]*Departments of Pediatrics/Cardiology and Bioengineering, Children's Hospital of Pittsburgh, PA, USA*
[d]*Department of Pediatrics/Cardiology, Children's Hospital of Philadelphia, PA, USA*

Accepted 11 March 2008

Abstract

This study focuses on the dynamic flow through the fetal aortic arch driven by the concurrent action of right and left ventricles. We created a parametric pulsatile computational fluid dynamics (CFD) model of the fetal aortic junction with physiologic vessel geometries. To gain a better biophysical understanding, an *in vitro* experimental fetal flow loop for flow visualization was constructed for identical CFD conditions. CFD and *in vitro* experimental results were comparable. Swirling flow during the acceleration phase of the cardiac cycle and unidirectional flow following mid-deceleration phase were observed in pulmonary arteries (PA), head-neck vessels, and descending aorta. Right-to-left (oxygenated) blood flowed through the ductus arteriosus (DA) posterior relative to the antegrade left ventricular outflow tract (LVOT) stream and resembled jet flow. LVOT and right ventricular outflow tract flow mixing had not completed until ~3.5 descending aorta diameters downstream of the DA insertion into the aortic arch. Normal arch model flow patterns were then compared to flow patterns of four common congenital heart malformations that include aortic arch anomalies. Weak oscillatory reversing flow through the DA junction was observed only for the Tetralogy of Fallot configuration. PA and hypoplastic left heart syndrome configurations demonstrated complex, abnormal flow patterns in the PAs and head-neck vessels. Aortic coarctation resulted in large-scale recirculating flow in the aortic arch proximal to the DA. Intravascular flow patterns spatially correlated with abnormal vascular structures consistent with the paradigm that abnormal intravascular flow patterns associated with congenital heart disease influence vascular growth and function.

Keywords: Cardiac development; Hemodynamics; CFD; Cardiovascular fluid dynamics; Congenital heart defects; Fetal circulation; Embryonic aortic arch

1. Introduction

The fetal aortic arch is formed by the great vessels of the human arterial circulation and functions as a conduit for multiple flow streams during fetal life. The fetal aortic arch has two inlets represented by the right and left ventricular outflow tracks (RVOT and LVOT), and distributes oxygenated blood from the placenta and deoxygenated blood from the fetus via two outlets represented by the ascending aorta and pulmonary arteries to the head-neck vessels and the descending aorta (DAo) (Brezinka, 2001; Long, 1990; Sadler, 2006). The fetal aortic arch is in constant transformation in order to optimally match the hemodynamic requirements of the growing embryo (Keller et al., 2007). The higher oxygen saturated blood from the placenta is diluted with deoxygenated blood through a series of mixing events, while maintaining preferential flow of higher saturated blood to the developing brain (Blackburn, 2006; Stock and Vacanti, 2001; Szwast and Rychik,

Abbreviations: CFD, computational fluid dynamics; CHD, congenital heart disease; DA, ductus arteriosus; DAo, descending aorta; HLHS, hypoplastic left heart syndrome; LVOT, left ventricular outflow tract; PA, pulmonary artery; PAT, pulmonary atresia; RVOT, right ventricular outflow tract; TOF, Tetralogy of Fallot..

*Corresponding author. Tel.: +1 412 268 3027; fax: +1 412 268 9807.
E-mail address: kpekkan@andrew.cmu.edu (K. Pekkan).

0021-9290/$ - see front matter © 2008 Elsevier Ltd. All rights reserved.
doi:10.1016/j.jbiomech.2008.03.013

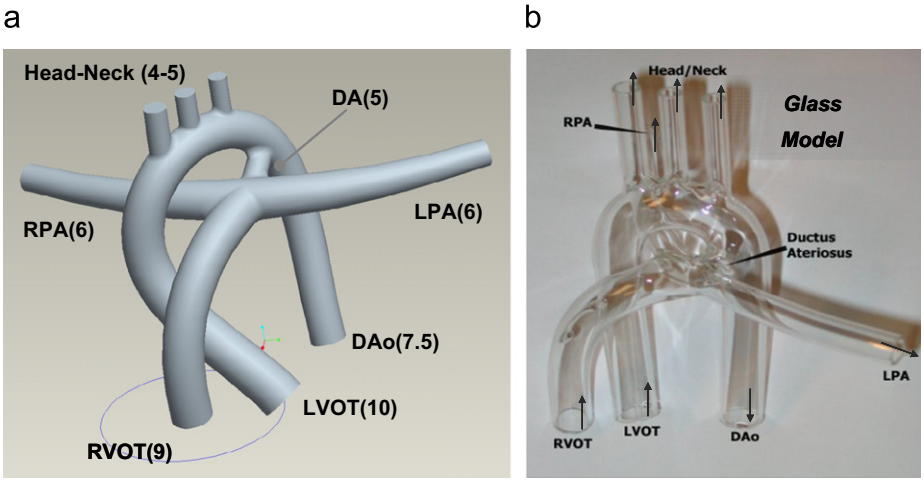

Fig. 1. Fetal aortic arch junction. The parametric solid computer aided design model in (a) with the normal vessel dimensions, given in parenthesis in millimeters. The glass replica of this model is shown in (b) which is used in flow visualization experiments. This idealized model has physiological vessel dimensions and flow rates for human fetus at late gestation (DA: ductus arteriosus, LVOT: left ventricular outflow tract, RVOT: right ventricular outflow tract, DAo: descending aorta, LPA: left pulmonary artery, RPA: right pulmonary artery). Vessel diameters (LVOT, RVOT, DA, PA, DAo) in mm used for congenital morphologies are as follows: HLHS (1.5, 12, 6, 10–7, 7.5), TOF (12, 5, 5, 8–5, 7.5) and PAT (0, 12, 5, 9–6, 7.5), respectively. Corresponding morphologies span a hypoplastic LVOT (HLHS) to a hypoplastic RVOT (PAT) (see also Fig. 7a).

2005). The fetal circulation (Allan et al., 2000; Huhta, 2001; Kiserud, 2005; Phoon, 2001) functions in a *fail-safe mode* where brain perfusion is "spared" in the setting of reduced antegrade aortic arch flow due to the presence of a parallel circulation with the capacity for retrograde perfusion via the ductus arteriosus (DA) (Fig. 1a). While the DA usually involutes spontaneously during the first week of life, a persistent DA is a common post-natal cardiovascular problem and may be essential for survival in the setting of some forms of congenital heart disease (CHD) (Frydrychowicz et al., 2007; Schneider and Moore, 2006). Patency of the DA can be maintained pharmacologically to support systemic and/or pulmonary blood flow in the setting of complex, cyanotic CHD where hypoplasia of the LVOT reduces antegrade aortic arch flow or hypoplasia of the RVOT reduces antegrade PA flow.

Cardiovascular solid mechanics and hemodynamic studies of cardiac development have predominantly focused on *early embryonic stages and ventricular flows* (Gleason et al., 2004; Nerurkar et al., 2006; Ramasubramanian et al., 2006). In 1928, Harvard University anatomist Bremer sketched the 3D spiral flow streams in fetal chick hearts at several developmental stages and highlighted the association between form and flow (Bremer, 1928). Systematic *in vivo* flow visualization confirmed these observations where CHDs reproducibly created via altered venous flow patterns (Hogers et al., 1995). Engineering fluid dynamic analysis tools have only recently supported the quantification of these observations. Pioneering fluid mechanics experiments performed by Gharib and co-workers (Forouhar et al., 2006; Hove et al., 2003) used high-frame rate confocal particle image velocimetry systems on zebrafish embryos and by Vennemann et al. (2006) used conventional microscopic particle image velocimetry techniques in chick embryos. Limited data is available using complementary computational fluid dynamics (CFD) analysis in the developing human heart. DeGroff et al. (2003) used postmortem micro-dissected human fetal ventricles at the pre- and post-looping stages (Pentecost et al., 2001) and Loots et al. (2003) used a simplified tubular heart model to perform CFD simulations. More recently, analysis of fluid-structure interactions in the outflow-tract (Rugonyi et al., 2007), active embryonic heart analytical models (Taber et al., 2007), and mechanical loading of the atrioventricular cardiac cushions (Butcher et al., 2007) in chick embryo have been presented. To our knowledge the hemodynamics of fetal aortic arch during mid-to-late gestation period has not been investigated in spite of its clear significance to perinatal/neonatal arch structure and function (Friedman and Fahey, 1993; Maeno et al., 1999) and the clinical management of patients with CHD (Cohen, 2001; Hoffman and Kaplan, 2002). Likewise, excellent previous studies have investigated the dynamics of the embryonic circulation through lumped parameter models (Pennati et al., 2003; Pennati and Fumero, 2000; Peskin, 1981; Yoshigi and Keller, 1997; Yoshigi et al., 2000); the main focus of the current study is to identify the large scale 3D flow structures and baseline governing flow physics using experimental flow visualization and CFD models for the normal fetal aortic arch and for great vessel flow patterns in the setting of selected major CHDs.

Hemodynamics of the normal adult-scale aorta is a classical topic of cardiovascular fluid dynamics (Caro et al., 1978; Fung, 1984; McDonald, 1974) and has been extensively studied (Jin et al., 2003; Leuprecht et al., 2003; Mori and Yamaguchi, 2002; Morris et al., 2005; Nakamura et al., 2006; Shahcheraghi et al., 2002; Suo, 2005; Wood et al., 2001). A detailed literature survey is provided in our recent work, where an *in vitro*/*in vivo*

validated, second-order accurate, transient CFD model of the neonatal aortic arch is developed (Pekkan et al., 2007a). Recent CFD models, focusing the normal mouse aortic-arch, revealed lower peak Reynolds and Womersley numbers (~250 and ~2) with significantly higher wall shear stress (Feintuch et al., 2007; Jin et al., 2007) compared to the human aorta, where low and oscillatory wall shear stress correlated with spatial protein expressions (Jin et al., 2007). Similarly, hemodynamics of the central PA tree has usually been studied *in isolation* (Hunter et al., 2006). Interestingly, the fetal aortic arch requires the *integration of both of these arterial systems* (pulmonary and systemic vascular beds driven by left and right hearts) in a single anatomical CFD domain due to its more complex parallel arrangement and challenging topology.

2. Methodology

2.1. Idealized anatomical model

A geometric model of the human fetal aortic arch representing the late gestation period (24–34 weeks) was created using computer-aided design software (Proengineer) (Fig. 1a). Anatomical dimensions and orientations were selected based on literature (Achiron et al., 2000; Long, 1990; Mielke and Benda, 2000b) and confirmed through interviews with three experienced pediatric cardiologists. The parametric nature enabled practical implementation of several suggested anatomical corrections.

Based on this computer-aided design model, a glass-blown replica was manufactured for use in *in vitro* experiments. Due to the technical challenges and complexity of the aortic junction in the glass model, all arteries had uniform average diameters with no taper, Fig. 1b.

To investigate abnormal hemodynamics, the normal parametric aortic arch model was modified to represent the great-vessel architectures of common CHD templates (Ilbawi et al., 2007; Wong et al., 2007); hypoplastic left heart syndrome (HLHS), Tetralogy of Fallot (TOF) and pulmonary atresia (PAT), see Fig. 1 caption for model dimensions.

2.2. Flow conditions

Non-dimensional numbers for great vessels are plotted as a function of the gestational age (Fig. 2; Long, 1990; Mielke and Benda, 2001). During late gestation, average heart rate is 143 bpm and cardiac outputs are 0.87 and 1.1 L/min through the LVOT and RVOT, respectively (Kiserud, 2005; Mielke and Benda, 2000a, 2001; Phoon, 2001). Flow waveforms used in this study are based on typical patient-specific aortic half-sine topology flow curves (Gadelha-Costa et al., 2007; Fig. 2). In the CFD model, no aortic backflow is specified for simplicity to avoid boundary condition type switching and to assure robust inflow boundary conditions however *in vitro* experiments are tuned to have this slight physiologic backflow through the set-up compliance.

For CHD templates, since the physiological RVOT and LVOT diameters are considerably different, as a first approximation, combined normal cardiac output is distributed between the LVOT and RVOT based on respective cross-sectional areas, with normal waveform topology and outflow split. Equal RPA and LPA flow was fixed at 50/50.

2.3. In vitro experimental studies—flow visualization

In the experimental flow loop, required physiological flow waveforms are created using a novel pumping arrangement in which a steady circulation pump and a pulsatile bulb pump is used in series. The bulb pump is driven through a pneumatic circuit that consists of a computer controlled pulse duplicator, compressor and solenoid valves (Leo et al., 2005). In the present arrangement, the pulsatile bulb pump was used solely to create the pulsatile flow component and had little effect on influencing the total flow rate, which was adjusted with the steady pump to the desired level generating the physiological flow waveform (Fig. 2). LVOT and RVOT flow rates are measured using ultrasonic clamp-on flow probes (Model T108, Transonic Inc., NY). Flow splitting between vessels was controlled using mechanical clamps and measured using bucket-and-stop-watch technique over a sufficient number of cardiac cycles (>150). Flow splits were first measured under steady average flow conditions, and verified again during pulsatile flow before flow visualization (~2.9% deviation from target flow splits, Table 1).

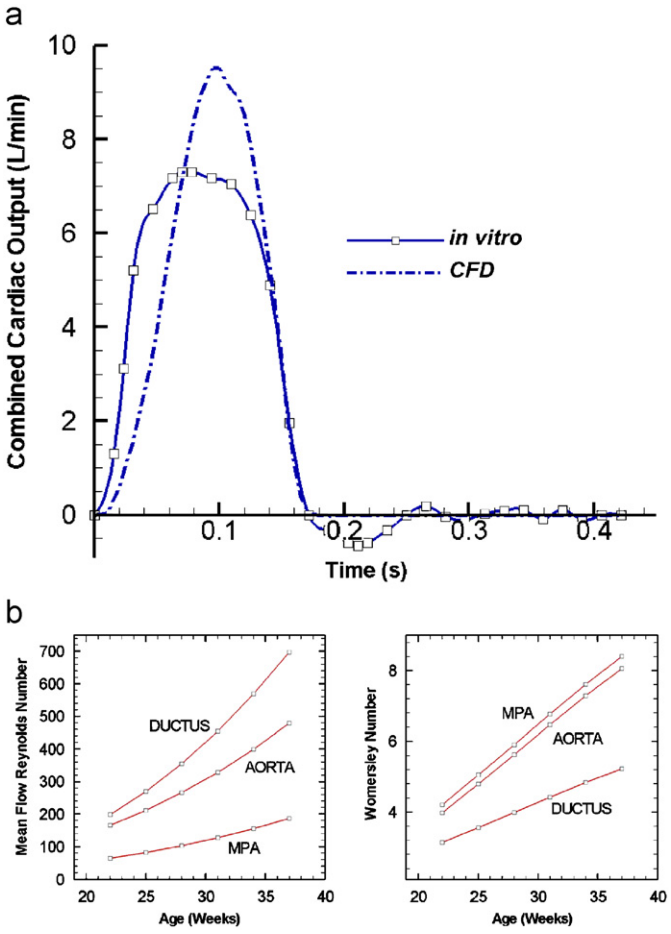

Fig. 2. (a) Computational and experimental flow waveforms specified and measured. The difference between these mean flow rates are less than 1%. CFD curve had no backflow. (b) Reynolds and Womersely numbers in major arterial vessels during late gestation. While the Reynolds numbers remain low due to the distributed total cardiac output between right and left hearts, unsteady effects are not negligible. Cardiac output data is abstracted from reference Gadelha-Costa et al. (2007).

In vitro cardiac gated flow visualizations are conducted using high-density prylolite particles and recorded with a high-speed CCD camera (A510, Basler AG, Ahrensburg) at 250 frames/s. Illumination was provided through a halogen lamp and CW red laser. Image analysis was performed to visualize particle traces and coherent structures from static flow visualization images as described earlier by Chrisohoides and Sotiropoulos (2003), which includes image background subtraction and consecutive image summing (2–4 depending on velocity).

2.4. Computational fluid dynamics

The computer-aided design model is meshed with three grid sizes. Results presented in the current manuscript correspond to the converged

fine grid size having a total of ~400,000 uniform tetrahedral elements (GAMBIT, Fluent Inc., Lebanon, NH). Flow fields were computed using the parallelized segregated finite-element CFD solver FIDAP (Fluent Inc.) utilizing a pressure projection algorithm both with the standard first-order and streamwise upwinding. For all runs, steady solution was used as the initial condition for subsequent transient computation. For well-developed inlet velocity profiles, the RVOT and LVOT cross-sections were extended. At outlets (head-neck vessels, DAo, LPA and RPA) one-diameter size auxiliary porous domains are employed to approximate the systemic and pulmonary resistance characteristics (Guadagni et al., 2001; Pekkan et al., 2005b). Standard pressure outlet conditions, as evaluated in Wang et al. (2007), for transient conditions, are adjusted one-diameter downstream of these porous beds to maintain the target mean physiological flow splits (LPA/RPA and head-neck/DAo). This CFD model has been utilized in earlier studies to understand fluid dynamics of complex CHDs and demonstrated good agreement with *in vitro* particle image velocimetry experiments (Pekkan et al., 2005c, 2007b; Zélicourt et al., 2005, 2006). Third-order convergence in time was achieved. Output time step was fixed at 0.001 s and the blood flow was assumed incompressible and Newtonian ($\rho = 1060\,\mathrm{kg\,m^{-3}}$, $\mu = 3.5 \times 10^{-3}\,\mathrm{Pa\,s}$). The vessel surfaces were treated as rigid and impermeable walls.

3. Results

3.1. Normal hemodynamics

3.1.1. Pulmonary artery flow

Flow during the acceleration phase is found to be unidirectional with little swirl. During the deceleration phase, both flow visualization experiments and CFD results demonstrated distinct swirling flow at the PAs, Fig. 3 and supplemental Movie 1. Steady mean flow conditions also featured distinct swirling flow within the PAs. In the steady flow particle tracking experiments, a flow separation line extending to the RPA is observed along the RVOT due to the curvature of the main PA (supplemental Movie 2).

Table 1
Typical flow distribution values that are maintained between the main vessels during *in vitro* flow visualization experiments

	HN (%)	LPA (%)	RPA (%)	Dao (%)
Steady split	13.9	7.3	7.2	71.6
Unsteady split	18.0	9.3	8.5	64.2
Target split	15.0	7.5	7.5	70.0

First the average target flow split is established at the steady flow condition (typical values provided in Row 1) which is verified again during the accompanying pulsatile (unsteady) flow experiments (Row 2) (HN: head-neck vessels, LPA: left pulmonary artery, RPA: right pulmonary artery, DAo: descending aorta).

3.1.2. Aortic arch

The aortic arch flow fields are presented in Fig. 4. Due to strong pulsatility, flow is highly uniform during acceleration phase however large recirculation patterns (indicating that flow breaking down due to instability) are observed during the deceleration phase, Movie 3. At the roots of all three head-neck vessels, during the deceleration phase, recirculation bubbles are observed. These flow structures are captured both in the CFD model and in experiments (Fig. 4).

3.1.3. Descending aorta

Similar and in phase with the PA flow patterns, swirling flows were observed in the DAo (supplemental Movie 4). These flow structures are spatially and temporally visualized both in the particle tracking experiments and in the CFD studies (Fig. 5).

3.1.4. Ductal right-to-left shunting

For the normal arch configuration, flow progressing through the RVOT preferentially flowed antegrade through the DA as well as into the LPA and RPA. DA shunt flow resembled a cross flow jet that stagnates at the outer wall of the DAo. RVOT and LVOT flows remain separated for ~3.5 DAo diameters within the DAo downstream of ductus (Fig. 6). Computational observations were confirmed using a black-dye injection into the RVOT, with the majority of the dye progressing preferentially through the DA (movies are not included for brevity).

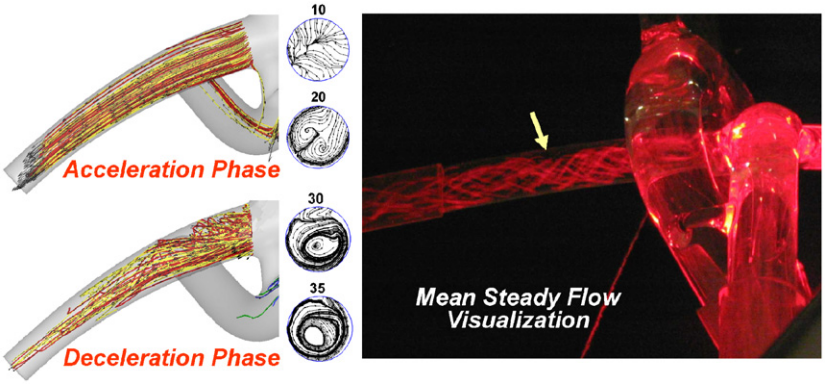

Fig. 3. Snapshots of pulmonary artery flow structures. Left: particle pathlines during acceleration and deceleration phases calculated from the pulsatile CFD results originating from a section at the LPA root are plotted. Middle: instantaneous streamlines are plotted for selected cardiac phases. Right: swirling flow visualized experimentally at the steady mean flow condition (see supplemental Movies 1 and 2).

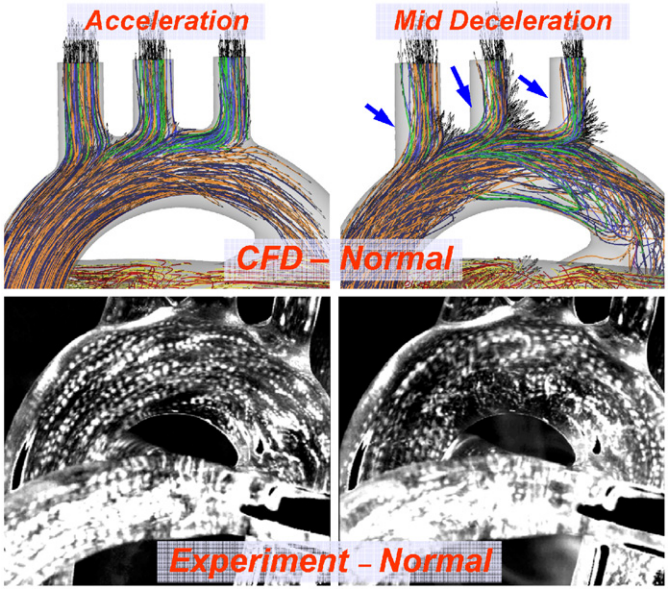

Fig. 4. Pulsatile flow visualization in the *normal* fetal aortic arch at acceleration and mid deceleration phases. Flow pathlines are plotted for both CFD and experiments for comparison at the same instant (see also supplemental Movie 3). During deceleration separation bubbles are observed for all head-neck vessels, highlighted with arrows.

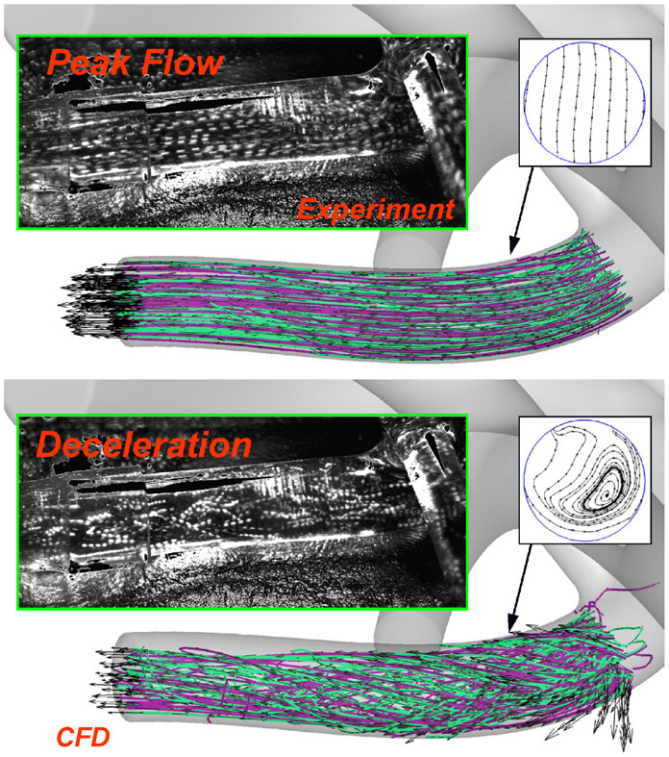

Fig. 5. Comparison of swirling flow patterns in the descending fetal aorta observed in CFD and *in vitro* experiments during the peak flow and mid-deceleration phases. Flow pathlines are visualized both for CFD computations and experiments. Cross-sectional flow streamlines are also shown as inserts featuring instant flow swirl.

3.2. Disease states

Results from the healthy aortic arch model allowed us subsequently to visualize and quantify the blood flow patterns of common CHDs at the bench-top. To our knowledge, biofluid dynamics visualization and quantification of these complex pathologies is novel.

3.2.1. Aortic coarctation downstream of ductus

Juxtaductal coarctation of the aorta is a common acyanotic malformation that is produced by narrowing of the aortic arch adjacent to the insertion of the DA and occurs in approximately 1 in 6000 live births (Zehr et al., 1995). When mild, this pathologic condition leads to upper-extremity hypertension and when severe this condition can result in LV failure and cardiovascular collapse. In order to approximate this fetal disease state on bench-top, a variable degree aortic coarctation was created proximal to the ductus using a balloon catheter inserted retrograde from the DAo. This configuration resulted low velocity large-scale flow recirculation spanning the second half of the aortic arch, just upstream of the ductus at all phases of the cardiac cycle. The 90% occlusion case in the supplemental Movie 5 can be compared with the healthy base line flow displayed in supplemental Movie 3.

3.2.2. Common congenital heart defects (abnormal DA flow patterns)

Pulsatile CHD velocity distributions are calculated along the two orthogonal planes intersecting the aortic arch junction (Fig. 7a and Movies (6–9)). In this manuscript, the DA flow patterns of different pathologies and flow curves during one cardiac cycle are compared, Fig. 7b. An oscillatory DA flow with reversing flow directions occurred only briefly for the TOF case, 6.9% of the total DA flow, during late systole due to the tight balance of relative RVOT and LVOT flow strengths. All other DA flows were either completely antegrade (PA to DAo) or completely retrograde (DAo to PA). For PAT and TOF, flow through the DA primarily supported pulmonary perfusion (DAo to PA), whereas in NORMAL and HLHS cases flow through the DA was primarily systemic (PA to DA). As expected, forward DA flow in the HLHS was almost double to that of the normal baseline condition since both the lower body and the head and neck were perfused via the DA. DA flow in PAT was higher than the normal pattern but in reverse direction, perfusing the pulmonary bed. Due to the typical "seagull" shape of the PAT stump, very complex 3D flow patterns are observed around the PA-DA intersection. During systole the DA jet swept the walls of the PA stump which created high wall shear stress particularly around the stump region, promoting further morphological remodeling of the PA's. For TOF and PAT cases PA swirl was recorded to be less than the NORMAL and HLHS. It must be emphasized that swirling flow within the PA leads to an order of magnitude higher wall shear stress and pressure drop (Pekkan et al., 2005a, b). Head-neck vessel perfusion

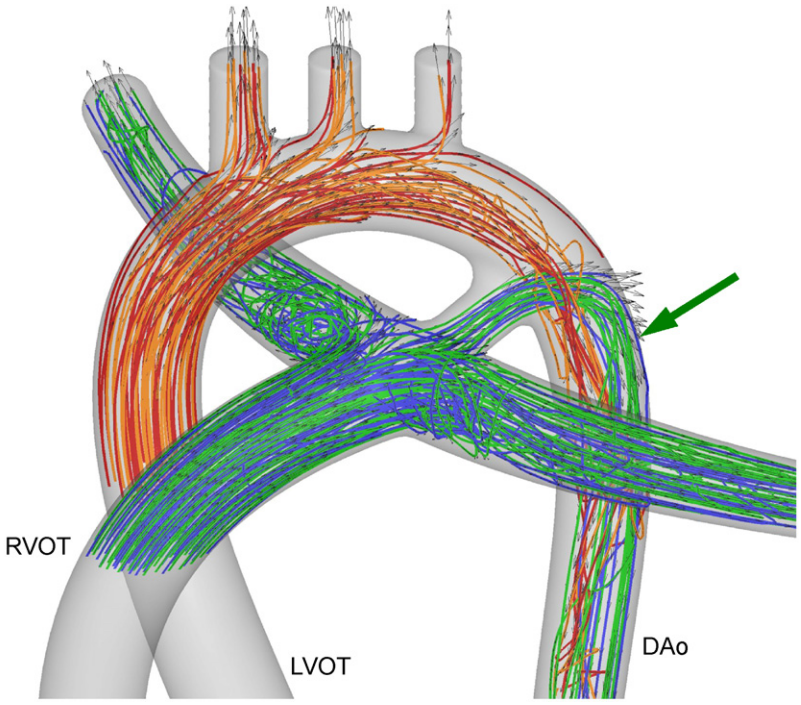

Fig. 6. Computed 3D flow streaklines illustrates the DA shunting orange- and green-labeled streams corresponds to LVOT and RVOT flows, respectively. RVOT and LVOT flows remain separated for a distance downstream of ductus as illustrated with the arrow.

in the HLHS case occurred in the retrograde direction altering the flow patterns in these vessels, forcing separation bubbles to the opposite ends of the vessels walls. The influence of these altered flow patterns on typical HLHS head-neck vessel abnormalities requires further investigation.

4. Discussion and conclusions

Recent advances in high-resolution ultrasound (Bonnet et al., 1999; Brackley et al., 2000; Cohen, 2001; Denkhaus and Winsberg, 1979; Hamar et al., 2006; Hecher et al., 1995; Tworetzky et al., 2001) and fetal cardiac MRI (Coakley, 2001; Fogel, 2006; Fogel et al., 2005; Hubbard and Harty, 1999; Liu et al., 2001) have demonstrated that aortic arch hemodynamics (Lenz and Chaoui, 2006) and great vessel anatomy (Axt-Fliedner et al., 2006; Hubbard and Harty, 1999) correlate with the prognosis of patients with complex CHD. However, fetal cardiac imaging modalities have practical limitations. Fetal echocardiography is often not a true 4D modality, has limited field-of-view, and is constrained by acoustic maternal and fetal windows. Likewise functional fetal MRI, which is now under development, has limitations due to dependence on fetal heart rate synchronization. For both techniques, fetal movement introduces significant image artifacts. Therefore, we developed an *in vitro* benchmark flow loop of the fetal circulation, specifically focusing on the fetal aortic arch configuration, to complement data derived from current fetal cardiac imaging modalities. These CFD studies also provide the opportunity to evaluate the impact of altered arch morphology and hemodynamics on mechanical loading of the developing heart across a range of developmental timepoints.

Due to the recognition that the growth of fetal cardiovascular structures correlates with antegrade blood flow and mechanical loading conditions, intrauterine aortic balloon valvuloplasty has emerged as a useful therapy for the fetus recognized to have aortic valve stenosis associated with reduced left ventricular function (Makikallio et al., 2006; Tierney et al., 2007; Tulzer et al., 2002). Successful fetal aortic valvuloplasty increases LVOT antegrade flow, is associated with both left ventricular and aortic arch growth, and has prevented the development of HLHS in some patients (Tometzki et al., 1999). Technical challenges (Emery et al., 2007) will eventually be solved and a new era will begin for the treatment of CHD that restores cardiovascular growth and remodeling prior to birth to reduce the severity of CHD (Gardiner, 2006; Rychik, 2005). The ability to visualize and model aortic arch and PA flow in the setting of CHD provides a valuable framework to quantify flow before and after fetal cardiac interventions and to quantify other emerging technologies for fetal therapy.

Combined with our recent study on neonatal aortic arch (Pekkan et al., 2007a) and the earlier biofluid dynamic studies of adult aortic arch, the hemodynamics of the human aorta can now be quantified throughout the entire biological timeline (fetal-to-adult) and changes in mechanical loading can be correlated with the large-scale vascular growth and remodeling. Peak Reynolds numbers for the fetal, neonatal, pediatric and adult aortas are 1063, 2984,

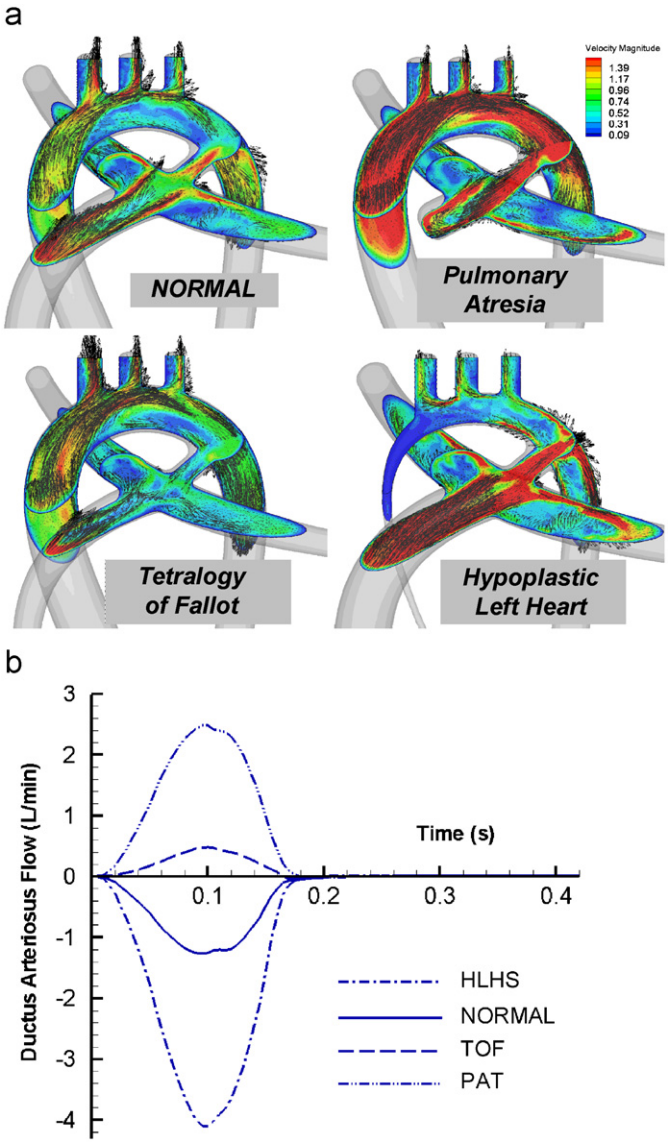

Fig. 7. (a) Instantaneous 3D fetal aortic flows of idealized CFD models of the normal and the three common congenital heart defect templates during mid-deceleration phase. Red and blue color corresponds to high and low flow velocities as graded in the upper right corner scale in m/s. Reversed and high DA flows for PAT and HLHS cases are illustrated. Flow fields over one cardiac cycle are provided in supplemental Movies (6–9). (b) Average flow waveforms calculated through the ductus arteriosus. Positive values indicate pulmonary perfusion. Only TOF featured a very weak backflow. All other cases were unidirectional (HLHS: hypoplastic left heart syndrome; TOF: Tetralogy of Fallot; and PAT: pulmonary atresia).

6812, and 4000–6000 (Ku, 1997; Stein and Sabbah, 1976), respectively. The fetal-to-neonatal transition is associated with a drastic increase in Reynolds number and mechanical loading, coincident with the closure of DA and almost doubling in aortic arch flow rates. The role of fluid mechanical forces on postnatal vascular growth and remodeling of the aortic arch and PAs is intriguing and requires further investigation. The inclusion of pressure and shear stress data at points throughout the normal and disease model geometries is required to fully understand the relationship between altered flow patterns, mechanical stresses, and changes in vessel architecture and growth. However, these data are beyond the scope of the current manuscript and will require the additional modeling of vessel wall properties to accurately represent deformations and stresses. These experiments are planned based on image, pressure, and velocity mapping experiments in both chick and mouse embryos.

Idealized parametric cardiovascular models have been successfully employed as a first approximation where 3D morphological and physiological data is incomplete and difficult to acquire (Liu et al., 2004; Politis et al., 2007). Fetal hemodynamics is one such set of conditions. The present study can be extended to subject-specific morphologies, with specified moving wall CFD once reliable temporal 4D *in vivo* data is available or FSI (through integration with ongoing structural studies on fetal ventricles (Tobita et al., 2005; Voronov et al., 2004)). Combination of an auxiliary porous domain with standard pressure boundary conditions produced a physiological outlet that is useful in transient computations. Based on our earlier experience with the standard outlet options (Liu et al., 2004; Wang et al., 2007), this type of boundary condition has captured the transient pulsatile flow swirl dynamics at all outlet branches adequately well. To simulate more accurate transients at the boundaries, the CFD model should be coupled to the lumped parameter models as presented in Lagana et al. (2005) and Migliavacca et al. (2006). Once all characteristics of the fetal circulation (ductus venosus and foramen ovale, etc.) are established these types of boundary conditions can be implemented. CFD simulations could be improved further by using the exact fetal blood properties, which are slightly different than the pediatric counterparts as employed in the present study.

The present manuscript is primarily on the *baseline* hemodynamic conditions present in the normal fetal aortic arch configuration. As demonstrated here, these results can be adapted to analyze different CHD paradigms and provide quantitative physiological information at different time-points during cardiovascular development. For each of the four disease states studied in this manuscript, comparable *in vivo* flow and pressure data in human fetuses is scarce. A recent MRI study provided detailed flow streamlines of a persistent DA (Frydrychowicz et al., 2007), which are qualitatively similar to those in our present study. Correlation of increased flow induced mechanical load with altered great vessel morphology can also be deduced from the present study. For example, larger HLHS DA diameters and smaller aortic arch diameters are consistent with visualized flows. Large-scale recirculation patterns in the aortic coarctation case likely correlated with altered vessel morphology. The reduced and reverse DA flow waveform of the TOF case correlates well with clinical observations. There is a generally accepted concept that growth of the central PA tree in TOF is determined by the degree of pulmonary valve stenosis and forward blood

flow, a similar concept is accepted for aortic valve flow and growth of the aortic arch. The PAT morphology represents another extreme state of DA flow where due to zero-diameter RVOT, DA flow is predominantly in the reverse direction. Detailed quantitative analysis, including vital organ perfusion characteristics of each of these four congenital cases is ongoing and planed to be presented in future clinical communications.

Conflict of interest

Authors have no conflict of interest in our manuscript titled "In vitro hemodynamic investigation of the human embryonic aortic arch".

Acknowledgments

This work is supported by an American Heart Association beginning-grant-in-aid, 0765284U and NIH BRP Grant HL67622. Mr. Nourparvar and Mr. Yerneni are supported through PURA (President's Undergraduate Research Awards). We also acknowledge the contributions of Drs. Shiva Sharma and W. James Parks in parametric CHD model development. Flow visualization is performed at Georgia Institute of Technology.

Appendix A. Supplementary materials

Supplementary data associated with this article can be found in the online version at doi:10.1016/j.jbiomech.2008.03.013.

References

Achiron, R., Zimand, S., Hegesh, J., Lipitz, S., Zalel, Y., Rotstein, Z., 2000. Fetal aortic arch measurements between 14 and 38 weeks' gestation: in-utero ultrasonographic study. Ultrasound in Obstetrics and Gynecology 15, 226–230.

Allan, L., Hornberger, L., Sharland, G., 2000. Textbook of Fetal Cardiology. Greenwich Medical Media Limited, London.

Axt-Fliedner, R., Kreiselmaier, P., Schwarze, A., Krapp, M., Gembruch, U., 2006. Development of hypoplastic left heart syndrome after diagnosis of aortic stenosis in the first trimester by early echocardiography. Ultrasound in Obstetrics and Gynecology 28, 106–109.

Blackburn, S., 2006. Placental, fetal, and transitional circulation revisited. Journal of Perinatal and Neonatal Nursing 20, 290–294.

Bonnet, D., Coltri, A., Butera, G., Fermont, L., Le Bidois, J., Kachaner, J., Sidi, D., 1999. Detection of transposition of the great arteries in fetuses reduces neonatal morbidity and mortality. Circulation 99, 916–918.

Brackley, K.J., Kilby, M.D., Wright, J.G., Brawn, W.J., Sethia, B., Stumper, O., Holder, R., Wyldes, M.P., Whittle, M.J., 2000. Outcome after prenatal diagnosis of hypoplastic left-heart syndrome: a case series. Lancet 356, 1143–1147.

Bremer, J.L., 1928. An interpretation of heart development. Journal of Anatomy 40, 307.

Brezinka, C., 2001. Fetal hemodynamics. Journal of Perinatal Medicine 29, 371–380.

Butcher, J.T., McQuinn, T.C., Sedmera, D., Turner, D., Markwald, R.R., 2007. Transitions in early embryonic atrioventricular valvular function correspond with changes in cushion biomechanics that are predictable by tissue composition. Circulation Research 100, 1503–1511.

Caro, C.G., Pedley, T.J., Schroter, R.C., Seed, W.A., 1978. The Mechanics of the Circulation. Oxford University Press, Oxford.

Chrisohoides, A., Sotiropoulos, F., 2003. Experimental visualization of Lagrangian coherent structures in aperiodic flows. Physics of Fluids 15, L25–L28.

Coakley, F.V., 2001. Role of magnetic resonance imaging in fetal surgery. Topics in Magnetic Resonance Imaging 12, 39–51.

Cohen, M.S., 2001. Fetal diagnosis and management of congenital heart disease. Clinical Perinatology 28, 11–29 v–vi.

DeGroff, C.G., Thornburg, B.L., Pentecost, J.O., Thornburg, K.L., Gharib, M., Sahn, D.J., Baptista, A., 2003. Flow in the early embryonic human heart: a numerical study. Pediatric Cardiology 24, 375–380.

Denkhaus, H., Winsberg, F., 1979. Ultrasonic measurement of the fetal ventricular system. Radiology 131, 781–787.

Emery, S.P., Kreutzer, J., Sherman, F.R., Fujimoto, K.L., Jaramaz, B., Nikou, C., Tobita, K., Keller, B.B., 2007. Computer-assisted navigation applied to fetal cardiac intervention. International Journal in Medical Robotics 3, 187–198.

Feintuch, A., Ruengsakulrach, P., Lin, A., Zhang, J., Zhou, Y.Q., Bishop, J., Davidson, L., Courtman, D., Foster, F.S., Steinman, D.A., Henkelman, R.M., Ethier, C.R., 2007. Hemodynamics in the mouse aortic arch as assessed by MRI, ultrasound, and numerical modeling. American Journal of Physiology—Heart and Circulatory Physiology 292, H884–H892.

Fogel, M.A., 2006. Cardiac magnetic resonance of single ventricles. Journal of Cardiovascular Magnetic Resonance 8, 661–670.

Fogel, M.A., Wilson, R.D., Flake, A., Johnson, M., Cohen, D., McNeal, G., Tian, Z.Y., Rychik, J., 2005. Preliminary investigations into a new method of functional assessment of the fetal heart using a novel application of 'real-time' cardiac magnetic resonance imaging. Fetal Diagnosis and Therapy 20, 475–480.

Forouhar, A.S., Liebling, M., Hickerson, A., Nasiraei-Moghaddam, A., Tsai, H.-J., Hove, J.R., Fraser, S.E., Dickinson, M.E., Gharib, M., 2006. The embryonic vertebrate heart tube is a dynamic suction pump. Science 312, 751–753.

Friedman, A.H., Fahey, J.T., 1993. The transition from fetal to neonatal circulation: normal responses and implications for infants with heart disease. Seminars in Perinatology 17, 106–121.

Frydrychowicz, A., Bley, T.A., Dittrich, S., Hennig, J., Langer, M., Markl, M., 2007. Visualization of vascular hemodynamics in a case of a large patent ductus arteriosus using flow sensitive 3D CMR at 3 T. Journal of Cardiovascular Magnetic Resonance 9, 585–587.

Fung, Y.C., 1984. Biodynamics: Circulation. Springer, New York.

Gadelha-Costa, A., Spara-Gadelha, P., Filho, F.M., Gadelha, E.B., 2007. Hemodynamic changes in the fetal arteries during the second half of pregnancy assessed by Doppler velocimetry. European Journal of Obstetrics and Gynecology Reproductive Biology 132, 148–153.

Gardiner, H.M., 2006. Keeping abreast of advances in fetal cardiology. Early Human Development 82, 415–419.

Gleason, R.L., Taber, L.A., Humphrey, J.D., 2004. A 2-D model of flow-induced alterations in the geometry, structure, and properties of carotid arteries. Journal of Biomechanical Engineering 126, 371–381.

Guadagni, G., Bove, E.L., Migliavacca, F., Dubini, G., 2001. Effects of pulmonary afterload on the hemodynamics after the hemi-Fontan procedure. Medical Engineering & Physics 23, 293–298.

Hamar, B.D., Dziura, J., Friedman, A., Kleinman, C.S., Copel, J.A., 2006. Trends in fetal echocardiography and implications for clinical practice: 1985–2003. Journal of Ultrasound in Medicine 25, 197–202.

Hecher, K., Campbell, S., Doyle, P., Harrington, K., Nicolaides, K., 1995. Assessment of fetal compromise by Doppler ultrasound investigation of the fetal circulation. Arterial, intracardiac, and venous blood flow velocity studies. Circulation 91, 129–138.

Hoffman, J.I., Kaplan, S., 2002. The incidence of congenital heart disease. Journal of American College of Cardiology 39, 1890–1900.

Hogers, B., DeRuiter, M.C., Baasten, A.M., Gittenberger-de Groot, A.C., Poelmann, R.E., 1995. Intracardiac blood flow patterns related to the yolk sac circulation of the chick embryo. Circulation Research 76, 871–877.

Hove, J.R., Koster, R.W., Forouhar, A.S., Acevedo-Bolton, G., Fraser, S.E., Gharib, M., 2003. Intracardiac fluid forces are an essential epigenetic factor for embryonic cardiogenesis. Nature 421, 172–177.

Hubbard, A.M., Harty, P., 1999. Prenatal magnetic resonance imaging of fetal anomalies. Seminars in Roentgenology 34, 41–47.

Huhta, J.C., 2001. Right ventricular function in the human fetus. Journal of Perinatal Medicine 29, 381–389.

Hunter, K.S., Lanning, C.J., Chen, S.Y., Zhang, Y., Garg, R., Ivy, D.D., Shandas, R., 2006. Simulations of congenital septal defect closure and reactivity testing in patient-specific models of the pediatric pulmonary vasculature: a 3D numerical study with fluid-structure interaction. Journal of Biomechanical Engineering 128, 564–572.

Ilbawi, A.M., Spicer, D.E., Bharati, S., Cook, A., Anderson, R.H., 2007. Morphologic study of the ascending aorta and aortic arch in hypoplastic left hearts: Surgical implications. The Journal of Thoracic and Cardiovascular Surgery 134, 99–105.

Jin, S., Oshinski, J., Giddens, D.P., 2003. Effects of wall motion and compliance on flow patterns in the ascending aorta. Journal of Biomechanical Engineering 125, 347–354.

Jin, S., Ferrara, D.E., Sorescu, D., Guldberg, R.E., Taylor, W.R., Giddens, D.P., 2007. Hemodynamic shear stresses in mouse aortas: implications for atherogenesis. Arteriosclerosis, Thrombosis and Vascular Biology 27, 346–351.

Keller, B.B., Liu, L.J., Tinney, J.P., Tobita, K., 2007. Cardiovascular developmental insights from embryos. Annals of the New York Academy of Sciences 1101, 377–388.

Kiserud, T., 2005. Physiology of the fetal circulation. Seminar of Fetal Neonatal Medicine 10, 493–503.

Ku, D.N., 1997. Blood flow in arteries. Annual Review of Fluid Mechanics 29, 399–434.

Lagana, K., Balossino, R., Migliavacca, F., Pennati, G., Bove, E.L., de Leval, M.R., Dubini, G., 2005. Multiscale modeling of the cardiovascular system: application to the study of pulmonary and coronary perfusions in the univentricular circulation. Journal of Biomechanics 38, 1129–1141.

Lenz, F., Chaoui, R., 2006. Changes in pulmonary venous Doppler parameters in fetal cardiac defects. Ultrasound in Obstetrics and Gynecology 28, 63–70.

Leo, H.L., Simon, H., Carberry, J., Lee, S.C., Yoganathan, A.P., 2005. A comparison of flow field structures of two tri-leaflet polymeric heart valves. Annals of Biomedical Engineering 33, 429–443.

Leuprecht, A., Kozerke, S., Boesiger, P., Perktold, K., 2003. Blood flow in the human ascending aorta: a combined MRI and CFD study. Journal of Engineering Mathematics 47, 387–404.

Liu, X., Ashtari, M., Leonidas, J.C., Chan, Y., 2001. Magnetic resonance imaging of the fetus in congenital intrathoracic disorders: preliminary observations. Pediatrics and Radiology 31, 435–439.

Liu, Y., Pekkan, K., Jones, C., Yoganathan, A.P., 2004. The effects of different mesh generation methods on fluid dynamic analysis and power loss in total cavopulmonary connection (TCPC). Journal of Biomechanical Engineering 126, 594–603.

Long, W., 1990. Fetal and Neonatal Cardiology. Saunders, Philadelphia.

Loots, E., Hillen, B., Veldman, A.E.P., 2003. The role of hemodynamics in the development of the outlow tract of the heart. Journal of Engineering Mathematics 45, 91–104.

Maeno, Y., Himeno, W., Fujino, H., Sugahara, Y., Furui, J., Mizumoto, Y., Kato, H., 1999. Progression of congenital heart disease in the prenatal period. Pediatrics International 41, 709–715.

Makikallio, K., McElhinney, D.B., Levine, J.C., Marx, G.R., Colan, S.D., Marshall, A.C., Lock, J.E., Marcus, E.N., Tworetzky, W., 2006. Fetal aortic valve stenosis and the evolution of hypoplastic left heart syndrome: patient selection for fetal intervention. Circulation 113, 1401–1405.

McDonald, D.A., 1974. Blood Flow in Arteries, second ed. Edward Arnold, London.

Mielke, G., Benda, N., 2000a. Blood flow velocity waveforms of the fetal pulmonary artery and the ductus arteriosus: reference ranges from 13 weeks to term. Ultrasound in Obstetrics and Gynecology 15, 213–218.

Mielke, G., Benda, N., 2000b. Reference ranges for two-dimensional echocardiographic examination of the fetal ductus arteriosus. Ultrasound in Obstetrics and Gynecology 15, 219–225.

Mielke, G., Benda, N., 2001. Cardiac output and central distribution of blood flow in the human fetus. Circulation 103, 1662–1668.

Migliavacca, F., Balossino, R., Pennati, G., Dubini, G., Hsia, T.Y., de Leval, M.R., Bove, E.L., 2006. Multiscale modelling in biofluidynamics: application to reconstructive paediatric cardiac surgery. Journal of Biomechanics 39, 1010–1020.

Mori, D., Yamaguchi, T., 2002. Computational fluid dynamics modeling and analysis of the effect of 3-D distortion of the human aortic arch. Computer Methods in Biomechanics and Biomedical Engineering 5, 249–260.

Morris, L., Delassus, P., Callanan, A., Walsh, M., Wallis, F., Grace, P., McGloughlin, T., 2005. 3-D numerical simulation of blood flow through models of the human aorta. Journal of Biomechanical Engineering 127, 767–775.

Nakamura, M., Wada, S., Yamaguchi, T., 2006. Computational analysis of blood flow in an integrated model of the left ventricle and the aorta. Journal of Biomechanical Engineering 128, 837–843.

Nerurkar, N.L., Ramasubramanian, A., Taber, L.A., 2006. Morphogenetic adaptation of the looping embryonic heart to altered mechanical loads. Development in Dynamics 235, 1822–1829.

Pekkan, K., Dasi, P., Wang, C., de Zelicourt, D., Sotiropoulos, F., Yoganathan, A., 2005a. Fluid flow and dissipation in intersecting counter-flow pipes, APS Division of Fluid Dynamics 58th Annual Meeting, Chicago.

Pekkan, K., Kitajima, H., Forbess, J., Fogel, M., Kanter, K., Parks, J.M., Sharma, S., Yoganathan, A.P., 2005b. Total cavopulmonary connection flow with functional left pulmonary artery stenosis—fenestration and angioplasty *in vitro*. Circulation 112, 3264–3271.

Pekkan, K., Zelicourt, D., Ge, L., Sotiropoulos, F., Frakes, D., Fogel, M., Yoganathan, A., 2005c. Physics-driven CFD modeling of complex anatomical cardiovascular flows—a TCPC case study. Annals of Biomedical Engineering 33, 284–300.

Pekkan, K., Dur, O., Kanter, K., Sundareswaran, K., Fogel, M., Yoganathan, A., Ündar, A., 2007a. Neonatal aortic arch hemodynamics and perfusion during cardiopulmonary bypass. Journal of Biomechanical Engineering, in press.

Pekkan, K., Dasi, L.P., de Zélicourt, D., Sundareswaran, K.S., Fogel, M.A., Kanter, K.R., Yoganathan, A.P., October, 2007b. Hemodynamic performance of stage-2 univentricular reconstruction: Glenn vs. hemi-Fontan templates. Annals of the Biomedical Engineering, in review.

Pennati, G., Fumero, R., 2000. Scaling approach to study the changes through the gestation of human fetal cardiac and circulatory behaviors. Annals of Biomedical Engineering 28, 442–452.

Pennati, G., Corno, C., Costantino, M.L., Bellotti, M., 2003. Umbilical flow distribution to the liver and the ductus venosus in human fetuses during gestation: an anatomy-based mathematical modeling. Medical Engineering and Physics 25, 229–238.

Pentecost, J.O., Sahn, D.J., Thornburg, B.L., Gharib, M., Baptista, A., Thornburg, K.L., 2001. Graphical and stereolithographic models of the developing human heart lumen. Computation of Medical Imaging Graph 25, 459–463.

Peskin, C., 1981. Changes in the circulation occurring at birth. In: Hoppensteadt, F. (Ed.), Lectures in Applied Mathematics, vol. 19. American Mathematical Society of Providence, pp. 9–19.

Phoon, C.K., 2001. Circulatory physiology in the developing embryo. Current Opinions on Pediatrics 13, 456–464.

Politis, A.K., Stavropoulos, G.P., Christolis, M.N., Panagopoulos, F.G., Vlachos, N.S., Markatos, N.C., 2007. Numerical modeling of

simulated blood flow in idealized composite arterial coronary grafts: steady state simulations. Journal of Biomechanics 40, 1125–1136.

Ramasubramanian, A., Latacha, K.S., Benjamin, J.M., Voronov, D.A., Ravi, A., Taber, L.A., 2006. Computational model for early cardiac looping. Annals of Biomedical Engineering 34, 1655–1669.

Rugonyi, S., Liu, A., Pentecost, J.O., Thornburg, K.L., 2007. Finite element modeling of blood flow-induced mechanical forces in the outflow tract of chick embryonic hearts. Computers & Structures 85, 727–738.

Rychik, J., 2005. Hypoplastic left heart syndrome: from in-utero diagnosis to school age. Seminars on Fetal Neonatal Medicine 10, 553–566.

Sadler, T., 2006. Langman's Medical Embryology, 10th ed. Lippincott Williams & Wilkins.

Schneider, D.J., Moore, J.W., 2006. Patent ductus arteriosus. Circulation 114, 1873–1882.

Shahcheraghi, N., Dwyer, H.A., Cheer, A.Y., Barakat, A.I., Rutaganira, T., 2002. Unsteady and three-dimensional simulation of blood flow in the human aortic arch. Journal of Biomechanical Engineering 124, 378–387.

Stein, P.D., Sabbah, H.N., 1976. Turbulent blood flow in the ascending aorta of humans with normal and diseased aortic valves. Circulation Research 39, 58–65.

Stock, U.A., Vacanti, J.P., 2001. Cardiovascular physiology during fetal development and implications for tissue engineering. Tissue Engineering 7, 1–7.

Suo, J., 2005. Investigation of blood flow patterns and hemodynamics in the human ascending aorta and major trunks of right and left coronary arteries using magnetic resonance imaging and computational fluid dynamics. Biomedical Engineering, PhD, Georgia Institute of Technology, Atlanta.

Szwast, A., Rychik, J., 2005. Current concepts in fetal cardiovascular disease. Clinical Perinatology 32, 857–875 viii.

Taber, L.A., Zhang, J., Perucchio, R., 2007. Computational model for the transition from peristaltic to pulsatile flow in the embryonic heart tube. Journal of Biomechanical Engineering 129, 441–449.

Tierney, E.S., Wald, R.M., McElhinney, D.B., Marshall, A.C., Benson, C.B., Colan, S.D., Marcus, E.N., Marx, G.R., Levine, J.C., Wilkins-Haug, L., Lock, J.E., Tworetzky, W., 2007. Changes in left heart hemodynamics after technically successful in-utero aortic valvuloplasty. Ultrasound in Obstetrics and Gynecology 30, 715–720.

Tobita, K., Garrison, J.B., Liu, L.J., Tinney, J.P., Keller, B.B., 2005. Three-dimensional myofiber architecture of the embryonic left ventricle during normal development and altered mechanical loads. Analytical RecA Discovery Molecular Cell Evolution Biology 283, 193–201.

Tometzki, A.J., Suda, K., Kohl, T., Kovalchin, J.P., Silverman, N.H., 1999. Accuracy of prenatal echocardiographic diagnosis and prognosis of fetuses with conotruncal anomalies. Journal of American College of Cardiology 33, 1696–1701.

Tulzer, G., Arzt, W., Franklin, R.C., Loughna, P.V., Mair, R., Gardiner, H.M., 2002. Fetal pulmonary valvuloplasty for critical pulmonary stenosis or atresia with intact septum. Lancet 360, 1567–1568.

Tworetzky, W., McElhinney, D.B., Reddy, V.M., Brook, M.M., Hanley, F.L., Silverman, N.H., 2001. Improved surgical outcome after fetal diagnosis of hypoplastic left heart syndrome. Circulation 103, 1269–1273.

Vennemann, P., Kiger, K.T., Lindken, R., Groenendijk, B.C.W., Stekelenburg-de Vos, S., ten Hagen, T.L.M., Ursem, N.T.C., Poelmann, R.E., Westerweel, J., Hierck, B.P., 2006. *In vivo* micro particle image velocity of blood-plasma in the embryonic avian heart. Journal of Biomechanics 39, 1191–1200.

Voronov, D.A., Alford, P.W., Xu, G., Taber, L.A., 2004. The role of mechanical forces in dextral rotation during cardiac looping in the chick embryo. Development in Biology 272, 339–350.

Wang, C., Pekkan, K., de Zelicourt, D., Horner, M., Parihar, A., Kulkarni, A., Yoganathan, A.P., 2007. Progress in the CFD modeling of flow instabilities in anatomical total cavopulmonary connections. Annals of Biomedical Engineering 35 (11), 1840–1856.

Wong, S.F., Ward, C., Lee-Tannock, A., Le, S., Chan, F.Y., 2007. Pulmonary artery/aorta ratio in simple screening for fetal outflow tract abnormalities during the second trimester. Ultrasound in Obstetrics and Gynecology 30, 275–280.

Wood, N.B., Weston, S.J., Kilner, P.J., Gosman, A.D., Firmin, D.N., 2001. Combined MR imaging and CFD simulation of flow in the human descending aorta. Journals in Magnetization Resonance Imaging 13, 699–713.

Yoshigi, M., Keller, B.B., 1997. Characterization of embryonic aortic impedance with lumped parameter models. American Journal of Physiology 273, H19–H27.

Yoshigi, M., Knott, G.D., Keller, B.B., 2000. Lumped parameter estimation for the embryonic chick vascular system: a time-domain approach using MLAB. Computer Methods and Programs in Biomedicine 63, 29–41.

Zehr, K.J., Marc Gillinov, A., Redmond, M., Greene, P.S., Kan, J.S., Gardner, T.J., Reitz, B.A., Cameron, D.E., 1995. Repair of coarctation of the aorta in neonates and infants: a thirty-year experience. Annals of Thoracic Surgery 59, 33–41.

Zelicourt, D., Pekkan, K., Wills, L., Kanter, K., Sharma, S., Fogel, M., Yoganathan, A.P., 2005. *In vitro* flow analysis of a patient specific intra-atrial TCPC. Annals of Thoracic Surgery 79, 2094–2102.

Zélicourt, D., Pekkan, K., Parks, W.J., Kanter, K., Fogel, M., Yoganathan, A.P., 2006. Flow study of an extra-cardiac connection with persistent left superior vena cava. The Journal of Thoracic and Cardiovascular Surgery 131, 785–791.